# Supplementary Information

# Bridge-rich and loop-less hydrogel networks through suppressed micellization of multiblock polyelectrolytes

Jihoon Han[1]†, Saeed Najafi[2,3]†, Jiwon Park[4], Jun Mo Koo[5], Jehan Kim[6], Taehun Chung[1], Im Kyung Han[1], Suhun Chae[7], Dong Woo Cho[7,9], Jinah Jang[7,8,9,11], Unyong Jeong[1], Eunji Lee[4], Glenn H. Fredrickson[3], Joan-Emma Shea[2,12*] and Youn Soo Kim[1,10,11*]

*To whom correspondence should be addressed

E-mail: shea@ucsb.edu

E-mail: ysookim@postech.ac.kr

## Table of Contents

## 1. Materials

*N,N*-dimethylacrylamide (DMA), 2-acrylamido-2-methylpropane sulfonic acid (AMPS), (3-acrylamidopropyl)trimethylammonium chloride solution (APTC), 2,2′-azobis(2-methylpropionamidine) dihydrochloride (V-50), 4-((((2-carboxyethyl)thio)carbonothioyl)thio)-4-cyanopentanoic acid (CETCPA), sodium nitrate ($NaNO_3$), sodium phosphate monobasic ($NaH_2PO_4$), sodium phosphate dibasic ($Na_2HPO_4$), and deuterium oxide ($D_2O$) were purchased from Sigma-Aldrich. Methanol (MeOH), sulfuric acid ($H_2SO_4$), and sodium hydroxide (NaOH) were purchased from Samchun chemical. All chemicals were used without further purification. AMPS was neutralized by NaOH before polymerization. Ultrapure water with a resistivity of 18.2 MΩcm (Direct-Q® 5UV; Merck Millipore) was utilized in all experiments. A Spectra/Por® 7 dialysis membrane with pre-treated RC tubing (molecular weight cut-off (MWCO): 10 kDa, diameter: 29 mm) was purchased from Spectrum® Laboratories.

## 2. Polymer structure

Polymer structures were designed to compare their gelation mechanisms. To increase the water contents in the prepared hydrogels, DMA of a neutral hydrophilic monomer was used. When polymers were mixed at a 1:1 ratio, poly(APTC) and poly(AMPS) were self-assembled to obtain crosslinks. The total degree of polymerisation (DP) of the designed tri-PEs was 1050. Two charged blocks with DP = 150 were located at the ends of the polymer chain, and a neutral block with DP = 750 was located in its middle. The designed penta-PEs had a total DP of 1050. Three neutral blocks with DP = 250 were placed at both ends and in the middle of the polymer chain, and two charged blocks with DP = 150 were located between the neutral blocks. Finally, the designed nona-PEs had a total DP of 1850. Their structure resembled that of the penta-PEs with a larger number of blocks.

### Synthesis of multiblock copolymers by RAFT polymerization

**Synthesis of poly(*N,N*-dimethylacrylamide (DMA)).** Phosphate buffer solution (6 mL, 10 mM, pH = 7), 4-((((2-carboxyethyl)thio)carbonothioyl)thio)-4-cyanopentanoic acid (CETCPA) (17.9 mg, 7.63 mM), DMA (1,375 mg, 1.81 M), and 2,2′-azobis(2-methylpropionamidine) dihydrochloride (V-50) (1.0 mg, 0.48 mM) were introduced into a 100-mL flask equipped with a magnetic stirrer bar and

sealed with a rubber septum to synthesize poly(DMA). The mixture was deoxygenated by freeze–pump–thaw cycling for more than three times, after which polymerization was performed at 70 °C using a temperature-controlled heating mantle followed by stirring at 60 rpm for 2 h to reach a nearly full conversion. A sample was extracted from the polymerization medium using a degassed syringe for $^1$H NMR and GPC analyses to determine the monomer conversion, $M_{n,GPC}$, and $Đ$ values.

**Synthesis of poly((3-acrylamidopropyl)trimethyl ammonium chloride (APTC)).** Phosphate buffer solution (6 mL, 10 mM, pH = 7), CETCPA (17.9 mg, 6.57 mM), APTC (1,805 mg, 0.98 M), and V-50 (3.5 mg, 1.46 mM) were introduced into a 100-mL flask equipped with a magnetic stirrer bar and sealed with a rubber septum to synthesize poly(APTC). The mixture was deoxygenated by freeze–pump–thaw cycling for more than three times, after which polymerization was performed at 70 °C using a temperature-controlled heating mantle followed by stirring at 60 rpm for 2 h to reach a nearly full conversion. A sample was extracted from the polymerization medium using a degassed syringe for $^1$H NMR and GPC analyses to determine the monomer conversion, $M_{n,GPC}$, and $Đ$ values.

**Synthesis of poly(2-acrylamido-2-methyl-1-propanesulfonic acid (AMPS)).** Phosphate buffer solution (6 mL, 10 mM, pH = 7), CETCPA (17.9 mg, 6.08 mM), AMPS (1,725 mg, 0.87 M), and V-50 (2.0 mg, 0.77 mM) were introduced into a 100-mL flask equipped with a magnetic stirrer bar and sealed with a rubber septum to synthesize poly(AMPS). The mixture was deoxygenated by freeze–pump–thaw cycling for more than three times, after which polymerization was performed at 70 °C using a temperature-controlled heating mantle followed by stirring at 60 rpm for 2 h to reach a nearly full conversion. A sample was extracted from the polymerization medium using a degassed syringe for $^1$H NMR and GPC analyses to determine the monomer conversion, $M_{n,GPC}$, and $Đ$ values.

**Synthesis of subsequent blocks.** For the subsequent block extension, the deoxygenated monomer, initiator, and solvent mixture were injected into the polymerization medium (the detailed conditions are listed in Supplementary Tables 1, 3, 5, and 7). The resultant mixture was polymerized at 70 °C using a temperature-controlled heating mantle followed by stirring at 60 rpm for 2 h to reach a nearly full conversion. Before each injection, a sample was extracted from the polymerization medium using

a degassed syringe for $^1$H NMR and GPC analyses to determine the monomer conversion, $M_{n,GPC}$ and $Đ$ values (see Supplementary Figs. 1 and 2 and Supplementary Tables 2, 4, 6 and 8).

## 3. NMR spectroscopy

$^1$H NMR spectra were recorded on a Bruker Avance III 500 spectrometer at 25 °C and frequency of 500 MHz. The delay time was set to 2.5 s. All polymer samples were prepared in $D_2O$. Chemical shift values ($\delta$) were reported in ppm and determined with respect to non-deuterated solvent residues as internal references.

**Determination of the monomer conversion.** For the multiblock copolymers, monomer conversions were determined by comparing the decrease in the integrated intensity of the vinyl protons ($\delta$ = 6.70–5.70 ppm) of the monomer with that of the *R* group protons ($\delta$ = 3.60–2.75 ppm) of the monomer and polymer after polymerization by $^1$H NMR.

**Determination of the $M_{n,th}$ value.** The theoretical number-average molar mass ($M_{n,th}$) was calculated as follows:

$$M_{n,th} = \frac{[M]_0 p M_M}{[CTA]_0} + M_{CTA}, \quad (1)$$

where $[M]_0$ and $[CTA]_0$ are the initial concentrations of the monomer and chain transfer agent, respectively, and $p$ is the monomer conversion determined by $^1$H NMR. $M_M$ and $M_{CTA}$ are the molar masses (g mol$^{-1}$) of the monomer and chain transfer agent, respectively.

## 4. GPC studies

Molar mass distributions were measured on a Shimadzu LC-20AD liquid chromatography system using dedicated columns for anionic and cationic polymers. For anionic polymers, an Agilent PL-aquagel-OH, 8 μm, MIXED-M column (300 × 7.5 mm) and Agilent PL-aquagel-OH, 8 μm, guard column (50 × 7.5 mm) were utilised. The mobile phase consisted of 90% 0.15 M $NaNO_3$ aqueous solution and 10% methanol. The flow rate was 1.0 mL min$^{-1}$ and temperature was 40 °C. The instrument was calibrated with low-dispersity poly(ethyleneoxide) standards (Scientific Polymer)

whose molar masses varied between 0.2 and 800 kg mol$^{-1}$. For cationic polymers, TOSOH TSKgel, 10 μm, G5000PWXL-CP column (300 × 7.8 mm) and TOSOH TSKgel, 13 μm, PWXL-CP guard column (40 × 6 mm) were used. The mobile phase consisted of 0.3 M $NaNO_3$ aqueous solution with pH = 3 adjusted by sulfuric acid. The flow rate was 1.0 mL min$^{-1}$ and the temperature was 40 °C. The instrument was calibrated with low-dispersity poly(ethyleneoxide) standards (Scientific Polymer) whose molar masses varied between 0.2 and 800 kg mol$^{-1}$. Analyte samples were filtered through a polyvinylidene fluoride membrane with 0.2-μm pores before injection. The experimental molar mass ($M_{n,GPC}$) and dispersity ($Đ$) values of the synthesised polymers were determined by conventional calibration using the LC Solution software with a known RI detector calibration constant.

## 5. Small-angle X-ray scattering fitting model

Small-angle X-ray scattering (SAXS) profiles of the 0.2 wt% tri-, penta-, and nona-PEC were reproduced by applying the form factor of a core–shell sphere and structure factor of a hard sphere. The scattered intensity was computed as $I(q) = \phi \cdot F(q) \cdot S(q)$, where $\phi$, $F(q)$, and $S(q)$ were the scale factor, form factor, and structure factor, respectively. The form factor for the core–shell sphere with a polydisperse core radius was defined as follows:

$$F(q) = \frac{1}{V_{sp}}\left[\frac{3 \times V_{core} \times (p_{core} - p_{shell}) \times \Phi(qR_{core})}{qR_{core}} + \frac{3 \times V_{shell} \times (p_{shell} - p_{solvent}) \times \Phi(qR_{shell})}{qR_{shell}}\right]^2 ,$$

$$\Phi(qR_x) = \frac{sinx - xcosx}{x^2},$$

where $V$ is the volume, $p$ is the scattering length density, and $R$ is the radius. The polydispersity of the core radius was taken into account using the Schulz distribution.

## 6. Cryogenic transmission electron microscopy (Cryo-TEM)

Tri-, penta-, and nano-PEC for cryo-TEM analysis were prepared at 21 ℃ with humidity of 100 % using a Vitrobot Mark IV (Thermo Fisher Scientific, Waltham, MA, USA). Samples (3.5 μL) were applied onto a UV-$O_3$-treated lacey carbon-supported copper grid and then blotted for 2–3 sec to remove an excess solution before rapid vitrification by plunge-freezing the grids into liquid ethane at its melting temperature (~ –183 ℃). Grids were transferred to a Gatan cryo stage and imaged using JEM-1400 (JEOL Ltd., Tokyo, Japan) operating at 120 kV equipped with a Gatan 914 cryo-holder

(Gatan Inc., Pleasanton, CA, USA). TEM images were recorded and analyzed using a Xarosa bottom-mounted CMOS camera (EMSIS GmbH, Münster, Germany) and RADIUS software (Olympus-SiS, Münster, Germany).

## 7. Coarse grained molecular dynamics simulation

We provide a minimalistic representation of the polyelectrolytes by employing an elastic polymer model. Our coarse-grained (CG) model, the PEs are described as a linear collection of monomers, every 10 successive molecules of the experiment PEs are represented by a single monomeric unit with diameter σ and charge *e* (elementary charge unit). Monomers are linked to the adjacent monomers along the chain by means of stiff covalent bonds featured by FENE potential.[S1, S2] All the monomers exclude each other through a repulsive Weeks-Chandler-Anderson (WCA) potential.[S3] The triplet subsequent monomers interact via bending potentials. The total potential energy of the system is given by $H = U_{WCA} + U_{FENE} + U_{bend} + U_{elec}$ . The WCA potential is given by: $U_{WCA} = \frac{1}{2}\sum_{(i,j),i\neq j}^{N} V(d_{i,j})$

$$V(r) = \begin{cases} 4\epsilon\left[\left(\frac{\sigma}{r}\right)^{12} - \left(\frac{\sigma}{r}\right)^{6} + \frac{1}{4}\right] & if \quad r < 2^{1/6}\sigma \\ 0 & otherwise \end{cases}$$

The FENE bond potential reads: $U_{FENE} = -\sum_{i=1}^{N-1} \frac{\kappa_{fene}}{2}\left(\frac{R_0}{\sigma}\right)^2 ln\left[1 - \left(\frac{d_{i,i+1}}{R_0}\right)^2\right]$, where $d_{i,i+1} = |\vec{r}_i - \vec{r}_{i+1}|$ is the distance between the *i* and *i* + *1* monomers, $R_0 = 1.5\sigma$ is the maximum bond length and $\kappa_{fene} = 30\epsilon$ is the FENE interaction strength; $\epsilon$ is LJ unit of energy. The bending potential is: $U_{bend} = \sum_{i=1}^{N-1} \kappa_{bend}(1 - cos\theta_i)$, $\theta_i$ is the bending angle of the *ith* monomer and $\kappa_{bend}$ is the bending stiffness, here we set $\kappa_{bend} = 0.5\epsilon$, that roughly mimics the persistent length of the PEs. The electrostatic interaction is given by Columbic potential with Debye-Hückel electrostatic screening[S4]: $U_{elec}(r) = \frac{1}{2}\sum_{(i,j),i\neq j}^{N} \frac{q_i\, q_j}{4\pi\epsilon_0\epsilon_r r} e^{-kr}$, where $q$ is the unit of elementary charge with vacuum permittivity $\epsilon_0$ and relative permittivity $\epsilon_r = 80$, repressing water dielectric constant; and the invers of the Debye length $k$ is set to 0.3σ.

The equilibrium MD simulations were carried out in NVT ensemble using LAMMPS package,[S5] in constant temperature with $k_B T = \varepsilon$, using LJ unit. The temperature of the model systems was maintained through the Nose–Hoover thermostat. For every system, we performed $10^6\tau$ long

simulation, an equilibration phase that covers $10^4\tau$ was also performed. We used time step $0.01\tau$ to integrate the equation of motion, and the analyses were carried out at every $100\tau$.

To corroborate the viscoelastic properties of PEs-PEC calculated from the experiment, we performed oscillatory non equilibrium (NE) CGMD simulations.[S6] We first perform NPT simulations of the condensates, where the pressure is maintained at $P = 0.0$ in LJ units, using Nose-Hoover barostat. Next, by employing the NVT/SLLOD ensemble,[S7] the equilibrated condensates were subjected to an oscillatory shear strain $\zeta(\omega, t) = \zeta_0 \sin(\omega t)$ at different frequencies $\omega$, $\zeta_0$is the stain amplitude, and the oscillatory shear $\alpha(\omega, t) = \alpha_0 \sin(\omega t + \delta)$ stress was measured as a function of time, $\alpha_0$ and $\delta$ are the stress amplitude and its phase shift, respectively. The storage $G' = \alpha_0 \cos(\delta)/\zeta_0$ and loss $G'' = \alpha_0 \sin(\delta)/\zeta_0$ moduli were then determined at every $\omega$. The complex viscosity is simply calculated as $\eta^*(\omega) = (G'^2 + G''^2)^{1/2}/\omega$.

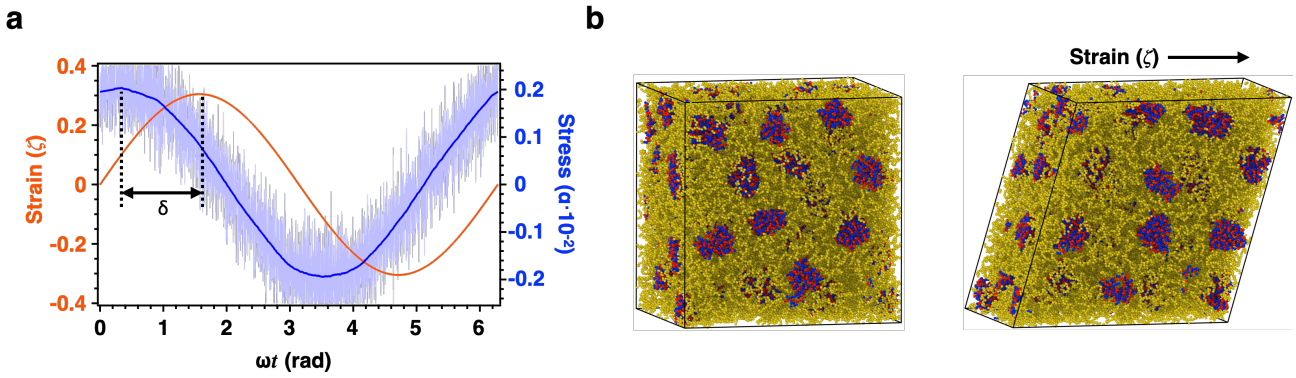


**Supplementary Figure NE-CGMD | Oscillatory shear non equilibrium molecular dynamics simulations**: **a**, The oscillatory strain $\zeta$ and the stress response $\alpha$ are shown; $\delta$ is the phase difference between the strain and stress. **b**, A representative illustration of the simulation box without and with strain.

In all NEMD simulations, the condensates were allowed to reach the steady state for 20 cycles. This steady state was then followed by the production NEMD runs, for which the oscillatory shear stress was carried out for more than 150 cycles at every frequency to ensure convergence.

## 8. Raman spectroscopy

Raman spectra were recorded in the range of 700-3,050 $cm^{-1}$ on Raman spectrometer (FEX-MD, NOST, South Korea) and 532 nm laser was used for sample excitation and total scan number of 3. Hydrogels having various concentrations were placed on a slide glass and measured. Laser power was 30 mW at a sample and time of a single measurement was 10 s.

## Two-dimensional correlation spectroscopy (2DCOS)

Two-dimensional correlation spectroscopy measurements were performed using the 2DShige program, and as a result, synchronous/asynchronous 2D correlation spectra were confirmed. In synchronous 2D Raman correlation spectrum, red autopeaks mean two correlated peaks change in same direction (increase or decrease together depending on increasing concentration), whereas blue crosspeaks mean two correlated peaks change in opposite direction. According to the Noda's rule, in asynchronous 2D Raman correlation spectrum, if two correlated peaks have the same color at the same position as the synchronous spectrum, the peak on the x-axis changes before the peak on the y-axis according to the change in concentration. If the colors are different, the peak on the y-axis changes before the peak on the x-axis according to the change in concentration.

## 9. Supplementary Figures 1–14

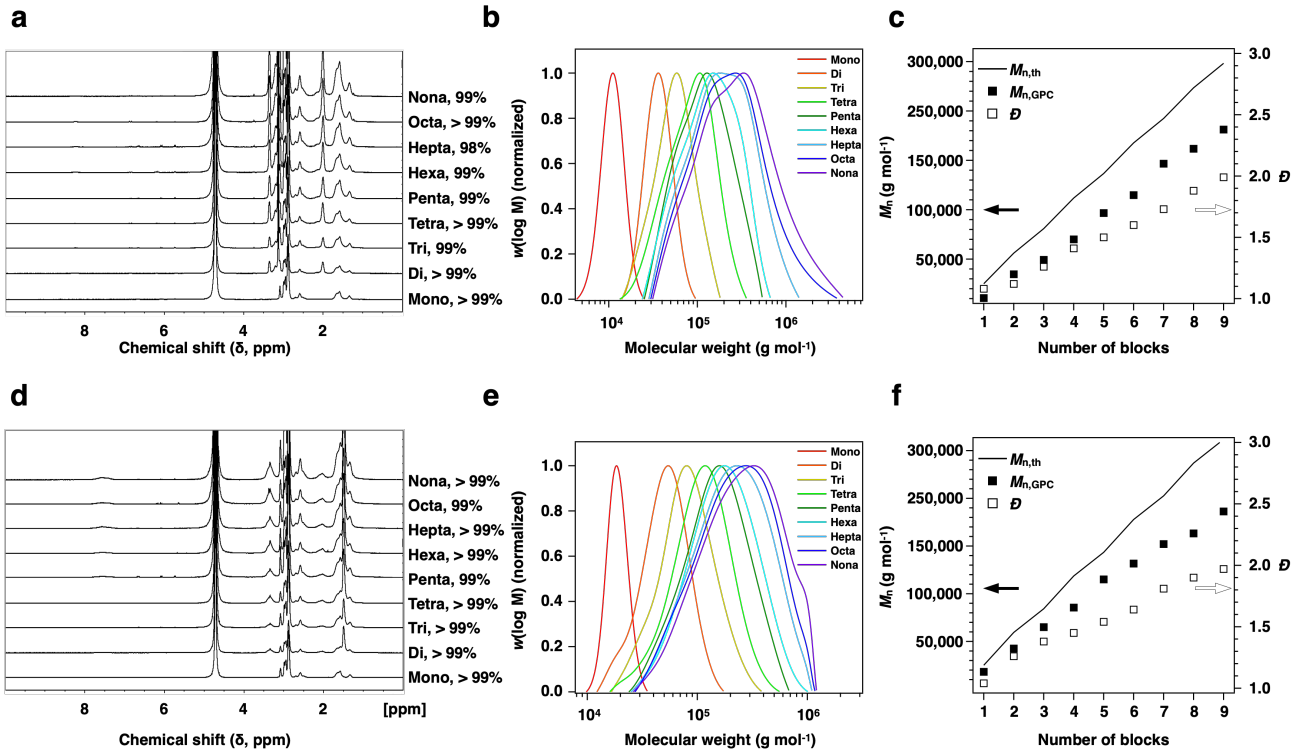


**Supplementary Figure 1 | Data analyses of penta-PEs and nona-PEs synthesized through a one-pot RAFT polymerization reaction.** **a**, $^{1}$H NMR spectra obtained for the consecutive block extensions of cationic PEs. The monomer conversion for each spectrum is >99%, and the right part lists sequential blocks. **b**, GPC traces of the molecular weight distributions determined for the consecutive block extensions. The y-axis title '*w*(logM)' represents the differential logarithmic molecular weight. **c**, Evolutions of the theoretical ($M_{n,th}$, black straight line) and experimental ($M_{n,GPC}$, black squares) number-average molar masses and dispersity values ($Đ$, open squares), as determined by GPC with the number of the synthesized blocks of cationic PEs. **d**, $^{1}$H NMR spectra recorded for the consecutive block extensions of anionic PEs. The monomer conversion for each spectrum is >99%, and the right part lists a number of sequential blocks. **e**, GPC traces of the molecular weight distributions obtained for the consecutive block extensions. **f**, Evolutions of the theoretical ($M_{n,th}$, black straight line) and experimental ($M_{n,GPC}$, black squares) number-average molar masses and dispersity values ($Đ$, open squares) determined by GPC with the number of the synthesized blocks of anionic PEs.

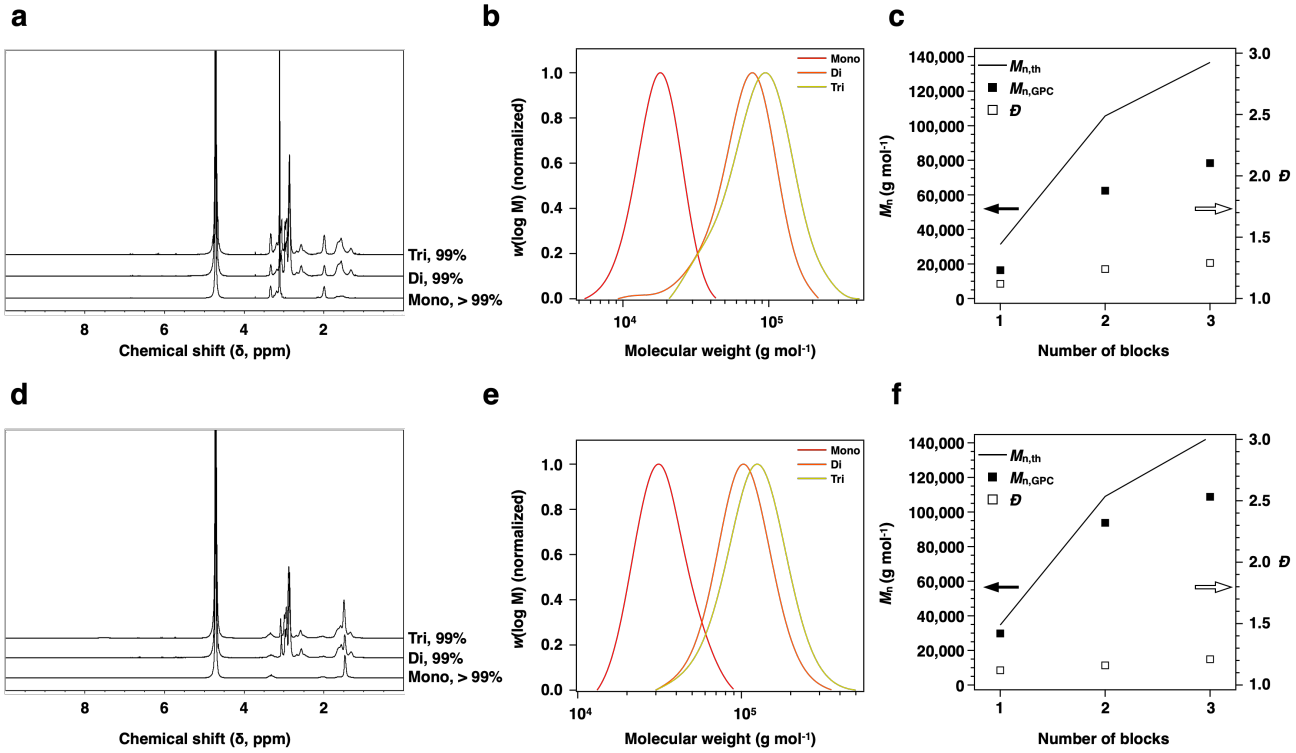


**Supplementary Figure 2 | Data analyses of the tri-PEs synthesized through a one-pot RAFT polymerization reaction. a**, $^{1}$H NMR spectra recorded for the consecutive block extensions of cationic PEs. The monomer conversion for each spectrum is >99%, and the right part lists sequential blocks. **b**, GPC traces of the molecular weight distributions obtained for the consecutive block extensions. The y-axis title '*w*(logM)' represents the differential logarithmic molecular weight. **c**, Evolutions of the theoretical ($M_{n,th}$, black straight line) and experimental ($M_{n,GPC}$, black squares) number-average molar masses and dispersity values ($Đ$, open squares) determined by GPC with the number of the synthesized blocks of cationic PEs. **d**, $^{1}$H NMR spectra recorded for the consecutive block extensions of anionic PEs. The monomer conversion for each spectrum is >99%, and the right part lists a number of sequential blocks. **e,** GPC traces of the molecular weight distributions obtained for the consecutive block extensions. **f**, Evolutions of the theoretical ($M_{n,th}$, black straight line) and experimental ($M_{n,GPC}$, black squares) number-average molar masses and dispersity values ($Đ$, open squares) determined by GPC with the number of the synthesized blocks of anionic PEs.

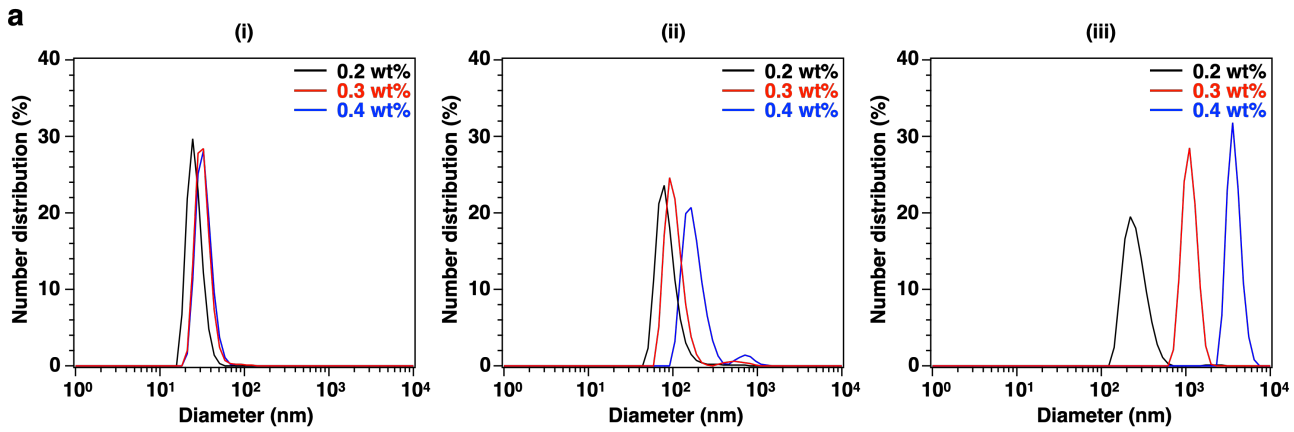


**Supplementary Figure 3 | a**, Size distributions of the self-assembled tri- (i), penta- (ii), and nona-PEC determined by DLS at polymer concentrations of 0.2 wt% (black), 0.3 wt% (red), and 0.4 wt% (blue).

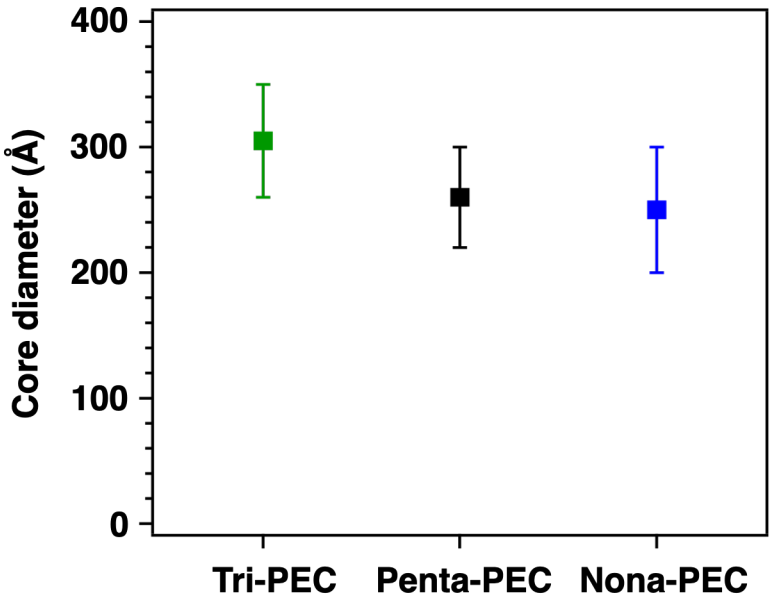


**Supplementary Figure 4 | Core diameter of tri-PEC (green closed rectangles), penta-PEC (black closed rectangle) and nona-PEC (blue closed rectangle) calculated from cryo-TEM images.**

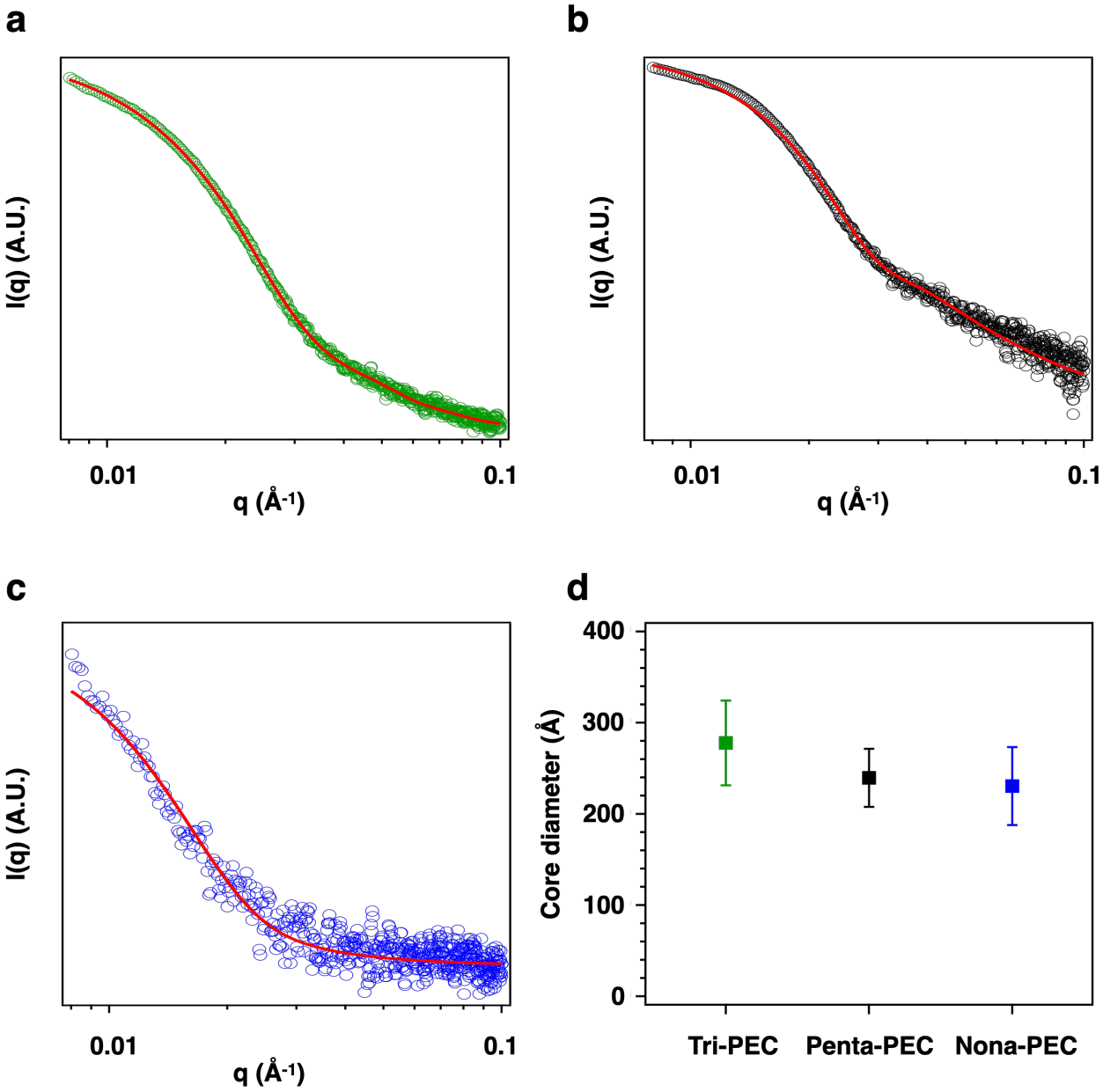


**Supplementary Figure 5 | SAXS profiles and calculated model fits of three different PEC.** SAXS profiles of tri-PEC (**a**, green open circles), penta-PEC (**b**, black open circles) and nona-PEC (**c**, blue open circles) with 0.2 wt% polymer concentration. All SAXS profiles were fitted by best model of the form factor of core-shell sphere and the structure factor of hard sphere (red solid line). **d**, Core diameter of tri-PEC (green closed rectangles), penta-PEC (black closed rectangle) and nona-PEC (blue closed rectangle).

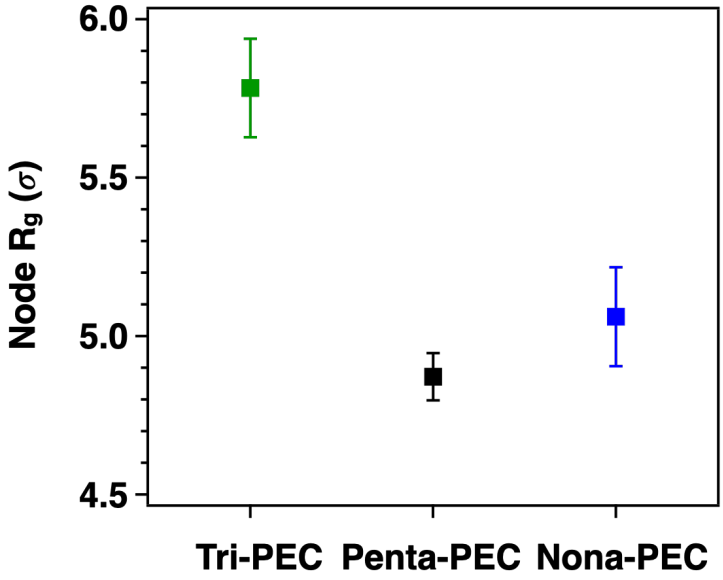


**Supplementary Figure 6** | Coacervate node radius of gyration ($R_g$) of tri-PEC (green closed rectangles), penta-PEC (black closed rectangle) and nona-PEC (blue closed rectangle) calculated from CG-MD simulations.

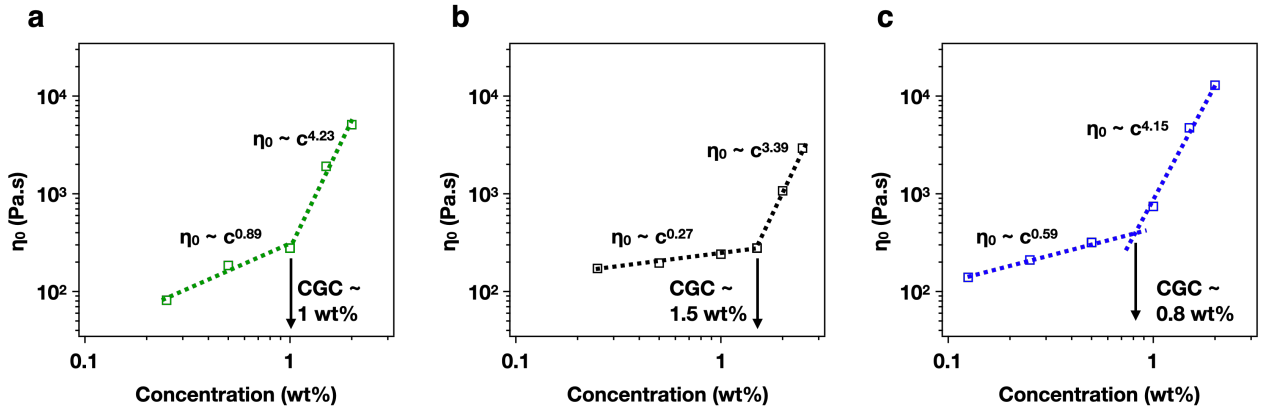


**Supplementary Figure 7 | Zero shear viscosity as a function of concentration for determining critical gelation concentration (CGC).** Tri-PEC (**a**, green open squares), penta-PEC (**b**, black open squares) and nona-PEC (**c**, blue open squares) hydrogels.

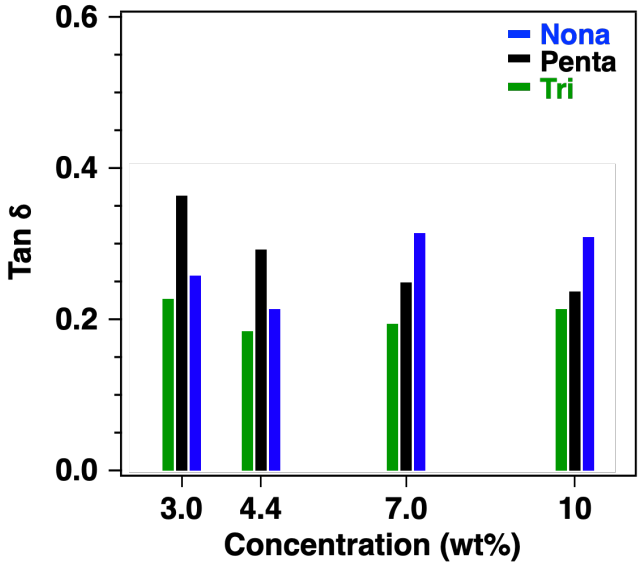


**Supplementary Figure 8 | Tan δ of three different PEC hydrogels at various polymer concentrations.** Tan **δ** (defined as G′′/G′) values obtained at strain amplitude sweep of a 1% strain.

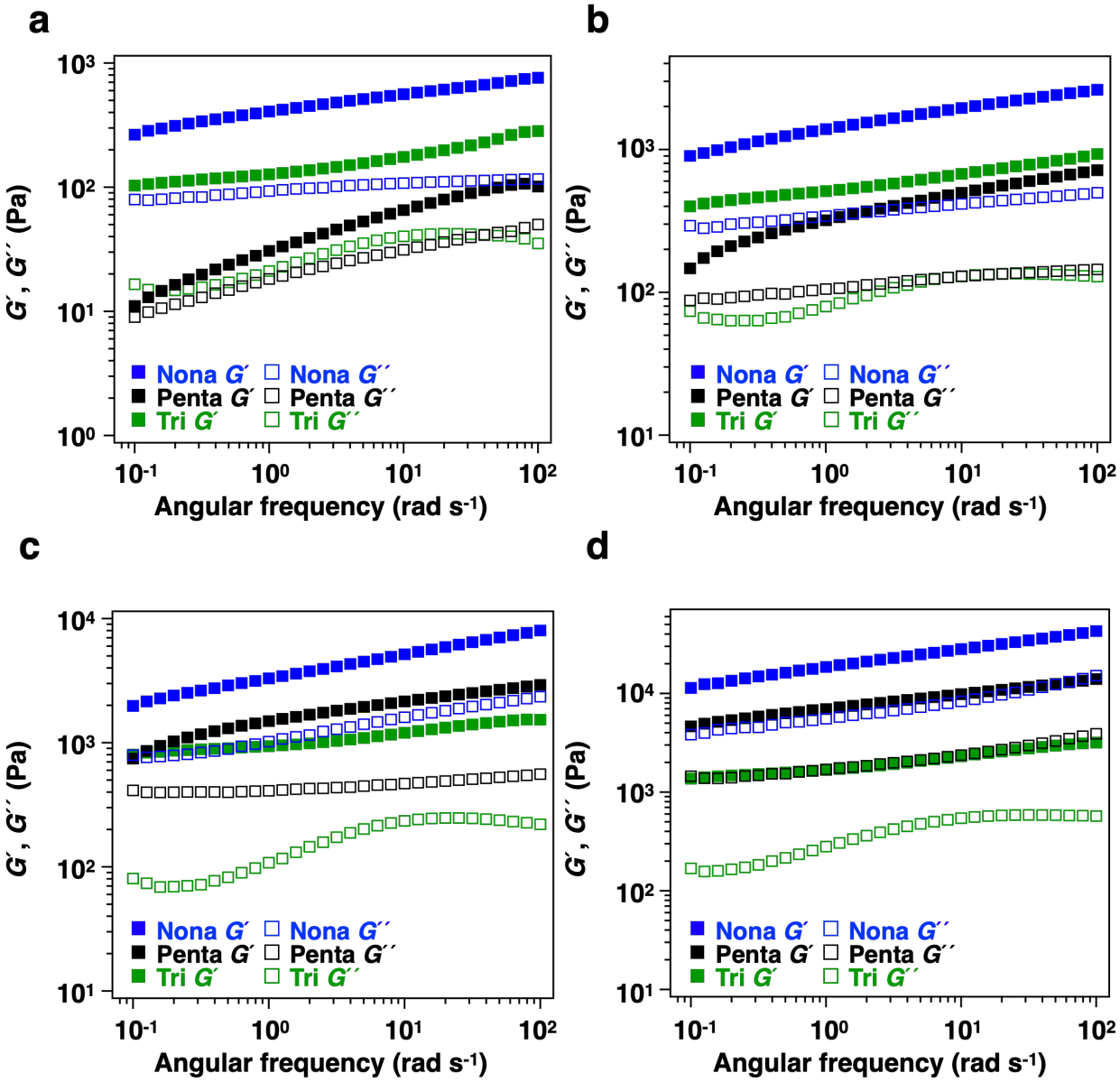


**Supplementary Figure 9 | Angular frequency dependencies of the storage (*G′*) and loss (*G″*) moduli of the three hydrogels.** Frequency sweep was performed in a range from 1 to 100 rad $s^{-1}$ at a strain of 1%. Storage (*G′*, closed rectangles) and loss (*G″*, open rectangles) moduli of the tri- (green), penta- (black), and nona-PEC (blue) hydrogels with 3.0 (**a**), 4.4 (**b**), 7.0 (**c**), and 10.0 wt% (**d**) polymer concentrations.

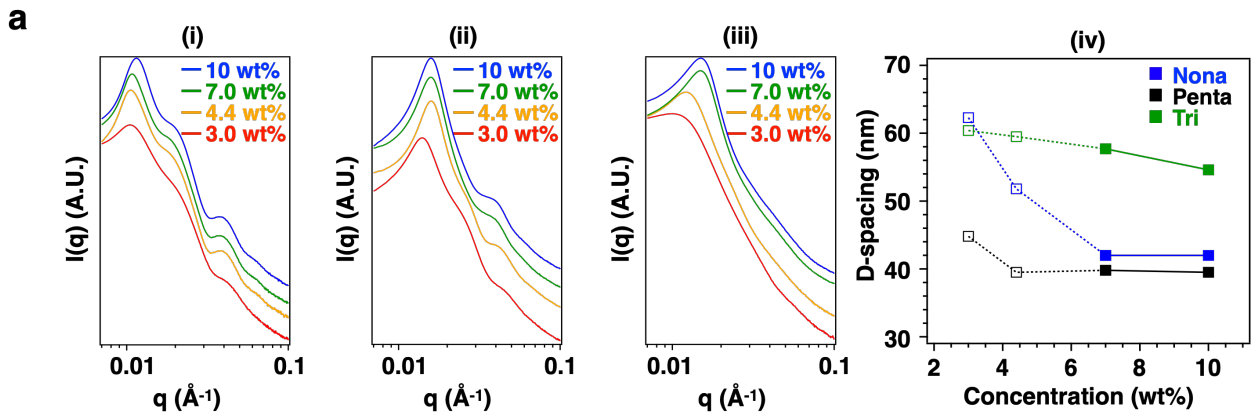


**Supplementary Figure 10 | SAXS profiles of the three types hydrogels. a**, SAXS profiles of tri- (i), penta- (ii), and nona-PEC (iii) hydrogels with 3.0 to 10.0 wt% polymer concentrations. The calculated domain spacing between the two cores with increasing polymer concentration (iv). Open squares represent low concentrations in which networks are not sufficiently connected, and closed squares represent high concentrations in which networks are sufficiently connected.

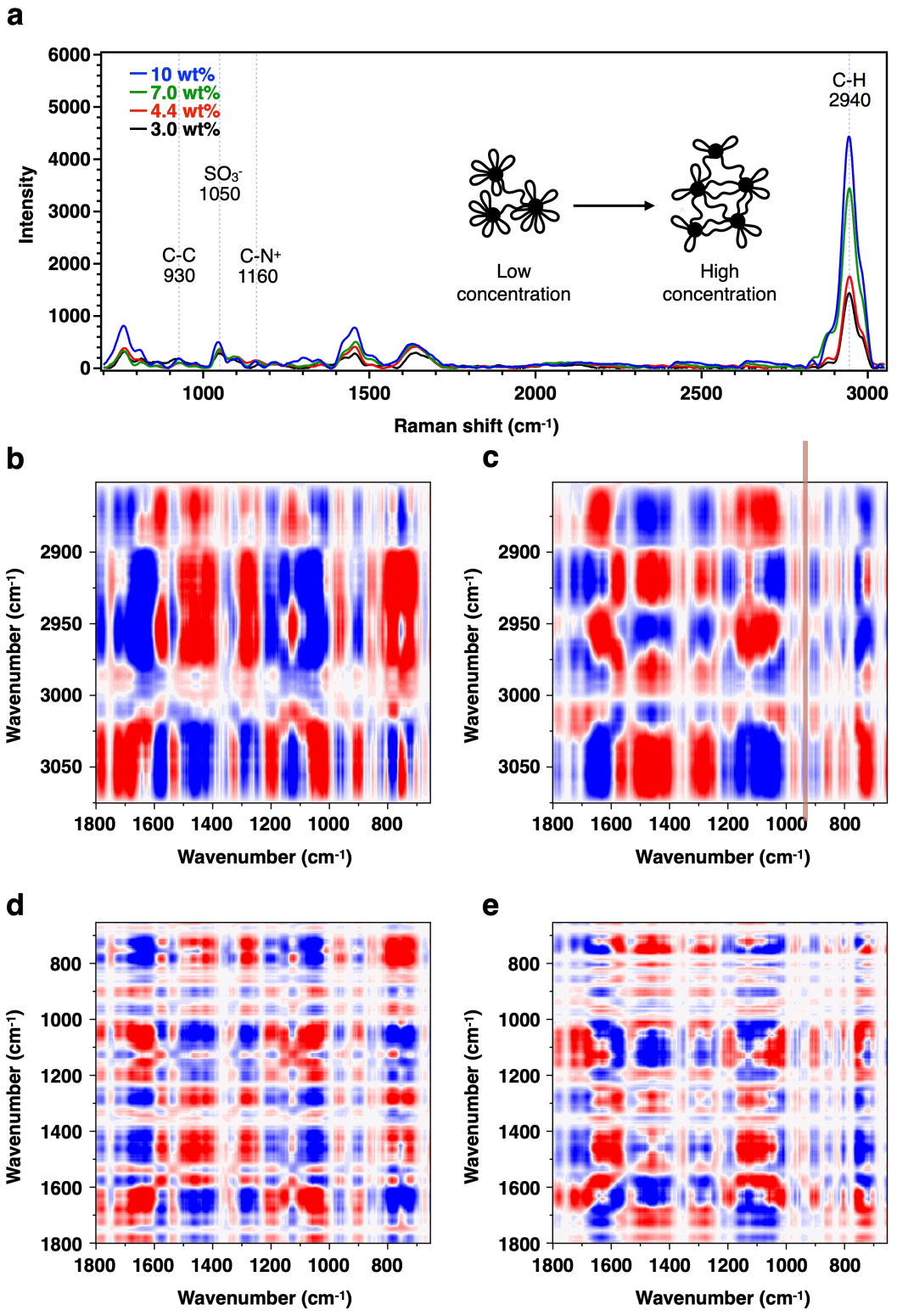


f

| Slow | | | Fast |
|---|---|---|---|
| 1160 | 1050 | 2940 | 930 |
| C–N+ | $SO_3^-$ | C-H | C-C |

**Supplementary Figure 11 | Concentration-dependent Raman spectral profiles of tri-PEC hydrogels and two-dimensional correlation spectroscopy (2D COS). a**, The Raman spectral profile (3,050-700 $cm^{-1}$) of tri-PEC hydrogels at concentrations of 3.0 to 10.0 wt%. Before 2DCOS analysis, all Raman spectra were area-normalized. **b**, Concentration-dependent synchronous 2D Raman correlation spectrum of tri-PEC from 1,800-650 $cm^{-1}$ to 3,075-2,850 $cm^{-1}$. **c**, Concentration-dependent asynchronous 2D Raman correlation spectrum of tri-PEC from 1,800-650 $cm^{-1}$ to 3,075-2,850 $cm^{-1}$. **d**, Concentration-dependent synchronous 2D Raman correlation spectrum of tri-PEC between 1,800-650 $cm^{-1}$. **e**, Concentration-dependent asynchronous 2D Raman correlation spectrum of tri-PEC between 1,800-650 $cm^{-1}$. **f**. Peak sequence of tri-PEC hydrogels according to concentration increase confirmed through 2DCOS analysis.

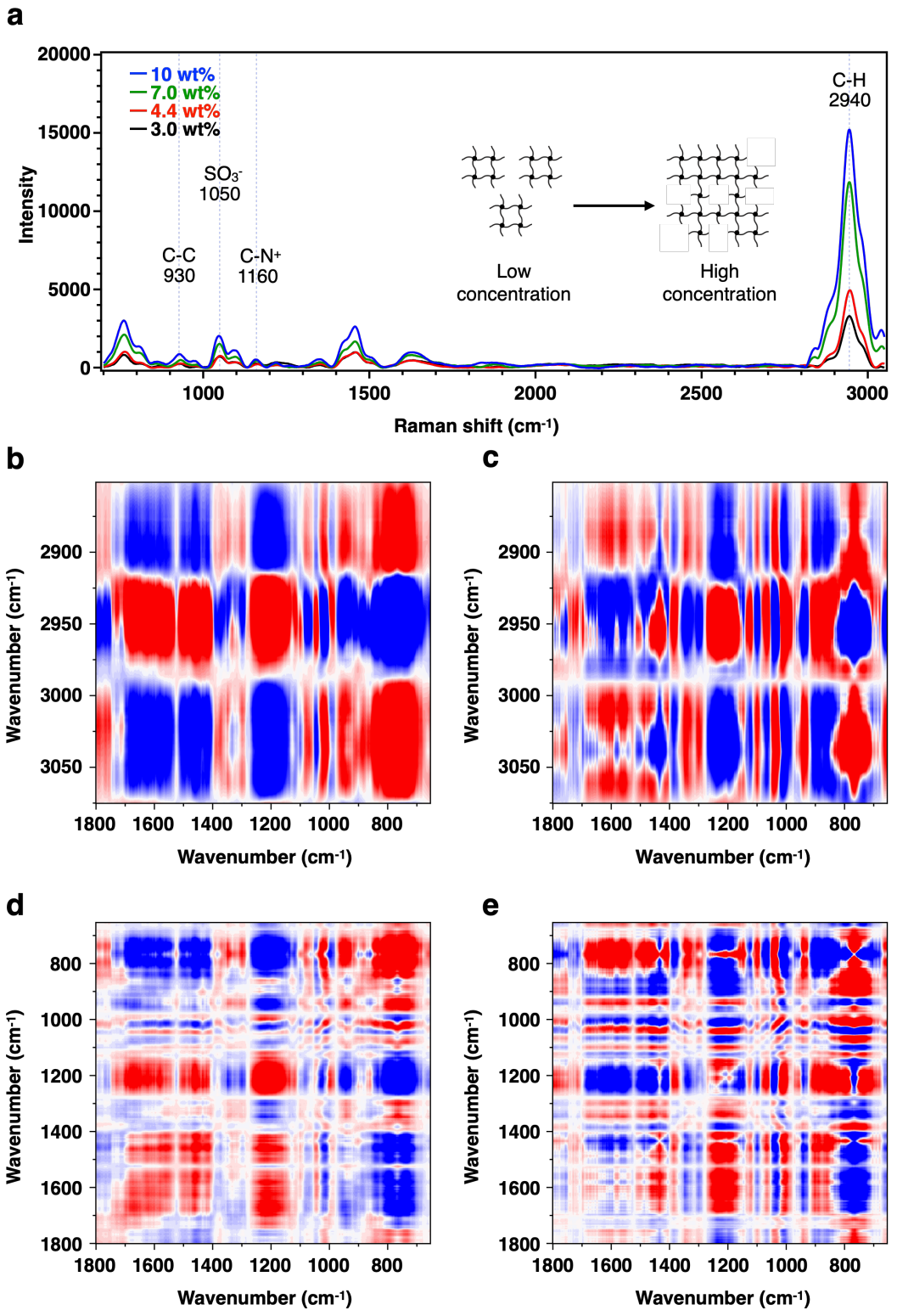


| Slow | | | Fast |
|---|---|---|---|
| 2940 | 930 | 1050 | 1160 |
| C-H | C-C | $SO_3^-$ | $C-N^+$ |

**Supplementary Figure 12 | Concentration-dependent Raman spectral profiles of penta-PEC hydrogels and two-dimensional correlation spectroscopy (2D COS). a,** The Raman spectral profile (3,050-700 $cm^{-1}$) of penta-PEC hydrogels at concentrations of 3.0 to 10.0 wt%. Before 2DCOS analysis, all Raman spectra were area-normalized. **b**, Concentration-dependent synchronous 2D Raman correlation spectrum of penta-PEC from 1,800-650 $cm^{-1}$ to 3,075-2,850 $cm^{-1}$. **c**, Concentration-dependent asynchronous 2D Raman correlation spectrum of penta-PEC from 1,800-650 $cm^{-1}$ to 3,075-2,850 $cm^{-1}$. **d**, Concentration-dependent synchronous 2D Raman correlation spectrum of penta-PEC between 1,800-650 $cm^{-1}$. **e**, Concentration-dependent asynchronous 2D Raman correlation spectrum of penta-PEC between 1,800-650 $cm^{-1}$. **f**. Peak sequence of penta-PEC hydrogels according to concentration increase confirmed through 2DCOS analysis.

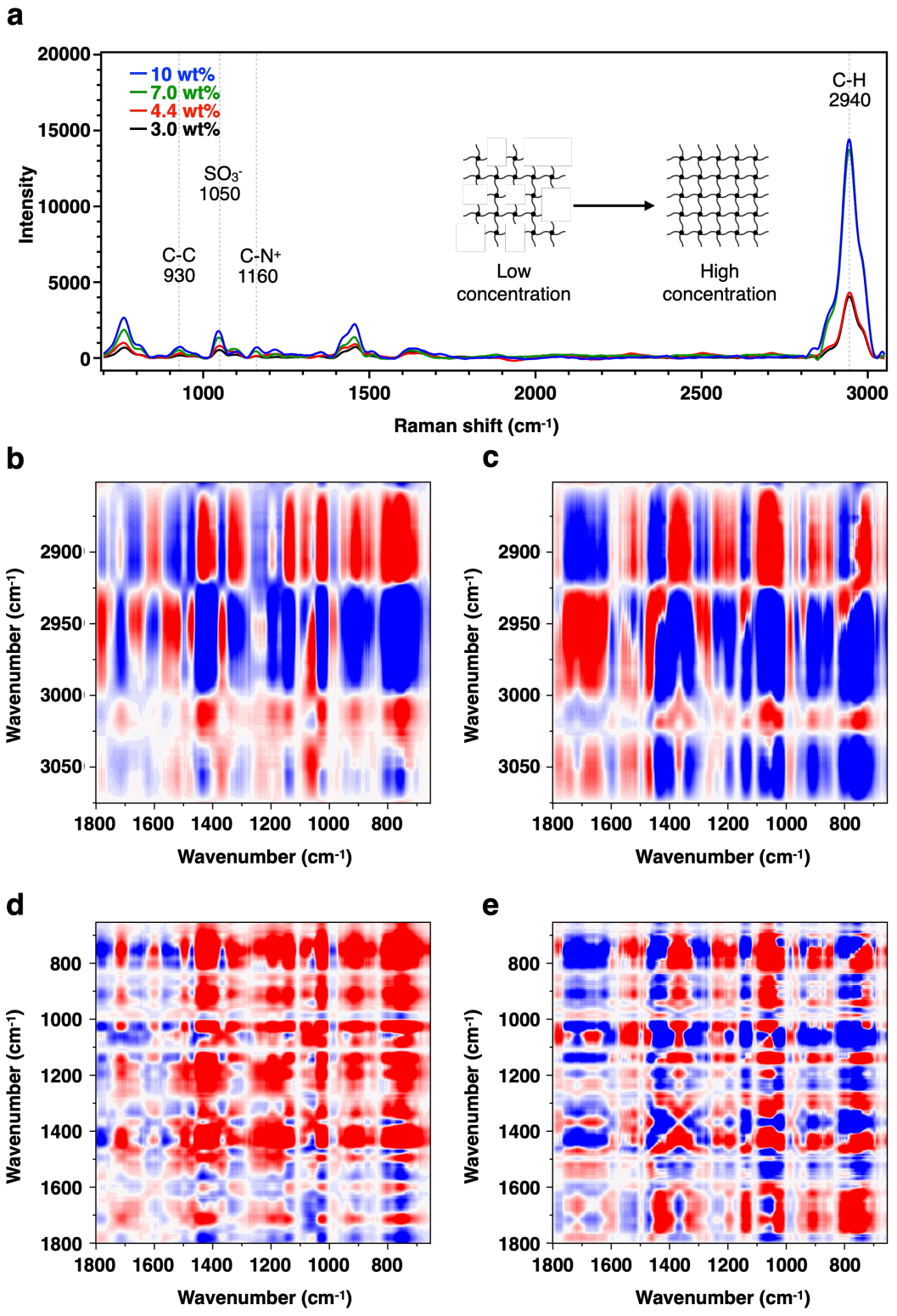


| Slow | | | Fast |
|---|---|---|---|
| 2940 | 930 | 1050 | 1160 |
| C-H | C-C | $SO_3^-$ | C-N+ |

**Supplementary Figure 13 | Concentration-dependent Raman spectral profiles of nona-PEC hydrogels and two-dimensional correlation spectroscopy (2D COS). a**, The Raman spectral profile (3,050-700 $cm^{-1}$) of nona-PEC hydrogels at concentrations of 3.0 to 10.0 wt%. Before 2DCOS analysis, all Raman spectra were area-normalized. **b**, Concentration-dependent synchronous 2D Raman correlation spectrum of nona-PEC from 1,800-650 $cm^{-1}$ to 3,075-2,850 $cm^{-1}$. **c**, Concentration-dependent asynchronous 2D Raman correlation spectrum of nona-PEC from 1,800-650 $cm^{-1}$ to 3,075-2,850 $cm^{-1}$. **d**, Concentration-dependent synchronous 2D Raman correlation spectrum of nona-PEC between 1,800-650 $cm^{-1}$. **e**, Concentration-dependent asynchronous 2D Raman correlation spectrum of nona-PEC between 1,800-650 $cm^{-1}$. **f**. Peak sequence of nona-PEC hydrogels according to concentration increase confirmed through 2DCOS analysis.

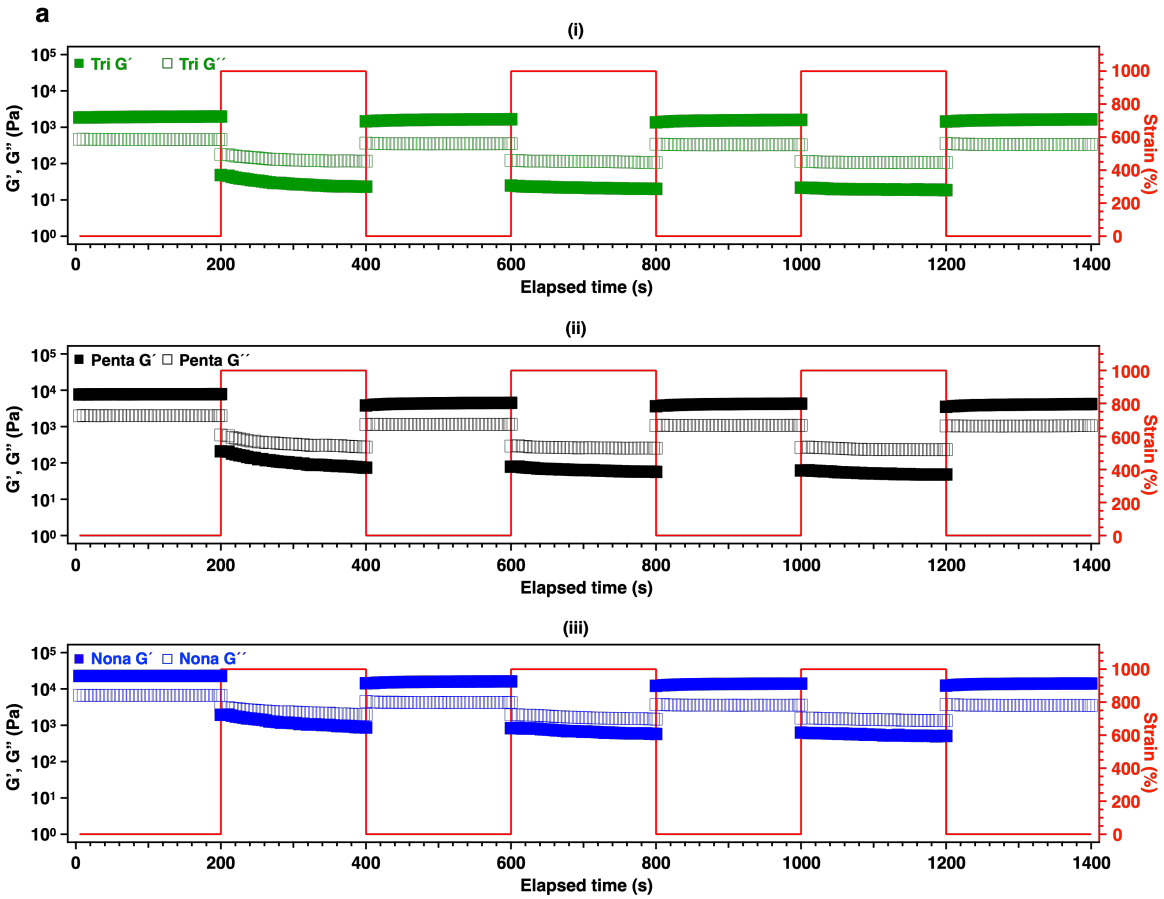


**Supplementary Figure 14 | Self-healing properties of the three PEC hydrogels. a**, Rheological properties of the tri- (green), penta- (black), and nona-PEC (blue) hydrogels with 10.0 wt% polymer concentrations. Cyclic strain jump tests were performed in a strain range from 1% to 1000% at a frequency of 3 rad $s^{-1}$. After the strain-induced failure (1000% strain), all hydrogels immediately and completely restored both their G′ (closed rectangles) and G′′ (open rectangles) values at a 1% strain.

## 10. Supplementary Tables 1–8

| Cycle | 1 | 2 | 3 | 4 | 5 | 6 | 7 | 8 | 9 |
|---|---|---|---|---|---|---|---|---|---|
| Monomer | DMA | APTC | DMA | APTC | DMA | APTC | DMA | APTC | DMA |
| $DP_{targeted}$ | 250 | 150 | 250 | 150 | 250 | 150 | 250 | 150 | 250 |
| $m_{Monomer\ added}$ (mg) | 1375 | 1805 | 1375 | 1805 | 1375 | 1805 | 1375 | 1805 | 1375 |
| $m_{CTA\ added}$ (mg) | 17.9 | - | - | - | - | - | - | - | - |
| $m_{V\text{-}50\ added}$ (mg) | 1 | 3.5 | 1.25 | 3.75 | 1.5 | 4 | 1.75 | 4.25 | 2 |
| $V_{PB\ added}$ (mL) | 6 | 3 | 2 | 3 | 2 | 3 | 2 | 3 | 2 |
| $V_{total}$ (mL)[a] | 7.63 | 14.819 | 18.499 | 25.738 | 29.468 | 36.757 | 40.537 | 47.876 | 51.706 |
| $m_{V\text{-}50\ total}$ (mg)[b] | 1 | 3.7 | 1.99 | 4.148 | 2.330 | 4.466 | 2.643 | 4.779 | 2.956 |
| $[V\text{-}50]_0$ (mol/L) | $4.83 \times 10^{-4}$ | $9.21 \times 10^{-4}$ | $3.97 \times 10^{-4}$ | $5.94 \times 10^{-4}$ | $2.92 \times 10^{-4}$ | $4.48 \times 10^{-4}$ | $2.40 \times 10^{-4}$ | $3.68 \times 10^{-4}$ | $2.11 \times 10^{-4}$ |
| $[Monomer]_0$ (mol/L) | 1.81 | 0.56 | 0.75 | 0.32 | 0.47 | 0.23 | 0.34 | 0.17 | 0.27 |
| $[CTA]_0$ / $[V\text{-}50]_0$ | 15.80 | 4.27 | 7.94 | 3.81 | 6.78 | 3.54 | 5.97 | 3.30 | 5.34 |

**Supplementary Table 1 | Preparation conditions of P(DMA$_{250}$-*b*-APTC$_{150}$-*b*-DMA$_{250}$-*b*-APTC$_{150}$-*b*-DMA$_{250}$) and P(DMA$_{250}$-*b*-APTC$_{150}$-*b*-DMA$_{250}$-*b*-APTC$_{150}$-*b*-DMA$_{250}$-*b*-APTC$_{150}$-*b*-DMA$_{250}$-*b*-APTC$_{150}$-*b*-DMA$_{250}$) synthesized via the one-pot RAFT polymerization in a 10-mM phosphate buffer solution at 70 °C with V-50 initiator (2 h per block).** [a] Represents the sum of the total volume of monomer + volume of initiator stock solution + volume of solvent + $V_{total}$ from the previous block. [b] $m_{v\text{-}50\ total}$ represents the sum of the initiator added $m_{v\text{-}50\ added}$ + the amount of initiator remaining from the previous block $m_{v\text{-}50\ remaining}$. ($m_{v\text{-}50\ remaining} = m_{v\text{-}50\ total} \times 2f e^{-kdt} \times (1\text{-}f_c/2)$ with $f = 0.5$, $f_c = 0$,[S8] $k_d = 1.21 \times 10^{-4}\ s^{-1}$.[S9]

| Block | Polymer | Monomer conversion[a] (%) | $M_{n,th}$[b] (g mol$^{-1}$) | $M_{n,GPC}$[c] (g mol$^{-1}$) | $Đ$[c] |
|---|---|---|---|---|---|
| 1 | Poly(DMA$_{250}$) | > 99 | 25,090 | 10,546 | 1.08 |
| 2 | Poly(DMA$_{250}$-*b*-APTC$_{150}$) | > 99 | 56,097 | 34,659 | 1.12 |
| 3 | Poly(DMA$_{250}$-*b*-APTC$_{150}$-*b*-DMA$_{250}$) | > 99 | 80,879 | 49,231 | 1.26 |
| 4 | Poly(DMA$_{250}$-*b*-APTC$_{150}$-*b*-DMA$_{250}$-*b*-APTC$_{150}$) | > 99 | 111,886 | 70,027 | 1.41 |
| 5 | Poly(DMA$_{250}$-*b*-APTC$_{150}$-*b*-DMA$_{250}$-*b*-APTC$_{150}$-*b*-DMA$_{250}$) | 99 | 136,668 | 96,625 | 1.50 |
| 6 | Poly(DMA$_{250}$-*b*-APTC$_{150}$-*b*-DMA$_{250}$-*b*-APTC$_{150}$-*b*-DMA$_{250}$-*b*-APTC$_{150}$) | > 99 | 167,675 | 114,803 | 1.60 |
| 7 | Poly(DMA$_{250}$-*b*-APTC$_{150}$-*b*-DMA$_{250}$-*b*-APTC$_{150}$-*b*-DMA$_{250}$-*b*-APTC$_{150}$-*b*-DMA$_{250}$) | > 99 | 192,457 | 146,588 | 1.73 |
| 8 | Poly(DMA$_{250}$-*b*-APTC$_{150}$-*b*-DMA$_{250}$-*b*-APTC$_{150}$-*b*-DMA$_{250}$-*b*-APTC$_{150}$-*b*-DMA$_{250}$-*b*-APTC$_{150}$) | 99 | 223,464 | 161,792 | 1.88 |
| 9 | Poly(DMA$_{250}$-*b*-APTC$_{150}$-*b*-DMA$_{250}$-*b*-APTC$_{150}$-*b*-DMA$_{250}$-*b*-APTC$_{150}$-*b*-DMA$_{250}$-*b*-APTC$_{150}$-*b*-DMA$_{250}$) | > 99 | 248,246 | 181,157 | 1.99 |

**Supplementary Table 2 | Final conversions, number-average molar masses, and dispersity values of P(DMA$_{250}$-*b*-APTC$_{150}$-*b*-DMA$_{250}$-*b*-APTC$_{150}$-*b*-DMA$_{250}$) and P(DMA$_{250}$-*b*-APTC$_{150}$-*b*-DMA$_{250}$-*b*-APTC$_{150}$-*b*-DMA$_{250}$-*b*-APTC$_{150}$-*b*-DMA$_{250}$-*b*-APTC$_{150}$-*b*-DMA$_{250}$) obtained in this study.** [a] Determined by $^1$H NMR. [b] Determined using eq (1). [c] Determined using GPC.

| Cycle | 1 | 2 | 3 | 4 | 5 | 6 | 7 | 8 | 9 |
|---|---|---|---|---|---|---|---|---|---|
| Monomer | DMA | AMPS | DMA | AMPS | DMA | AMPS | DMA | AMPS | DMA |
| $DP_{targeted}$ | 250 | 150 | 250 | 150 | 250 | 150 | 250 | 150 | 250 |
| $m_{Monomer\ added}$ (mg) | 1375 | 1725 | 1375 | 1725 | 1375 | 1725 | 1375 | 1725 | 1375 |
| $m_{CTA\ added}$ (mg) | 17.9 | - | - | - | - | - | - | - | - |
| $m_{V\text{-}50\ added}$ (mg) | 1 | 2 | 1.25 | 2.25 | 1.5 | 2.5 | 1.75 | 2.75 | 2 |
| $V_{PB\ added}$ (mL) | 6 | 3 | 2 | 3 | 2 | 3 | 2 | 3 | 2 |
| $V_{total}$ (mL)[a] | 7.63 | 14.195 | 17.858 | 24.473 | 28.203 | 34.868 | 38.648 | 45.363 | 49.193 |
| $m_{V\text{-}50\ total}$ (mg)[b] | 1 | 2.2 | 1.69 | 2.588 | 2.017 | 2.903 | 2.33 | 3.216 | 2.643 |
| $[V\text{-}50]_0$ (mol/L) | $4.83 \times 10^{-4}$ | $5.71 \times 10^{-4}$ | $3.49 \times 10^{-4}$ | $3.90 \times 10^{-4}$ | $2.64 \times 10^{-4}$ | $3.07 \times 10^{-4}$ | $2.22 \times 10^{-4}$ | $2.61 \times 10^{-4}$ | $1.98 \times 10^{-4}$ |
| $[Monomer]_0$ (mol/L) | 1.81 | 0.58 | 0.78 | 0.34 | 0.49 | 0.24 | 0.36 | 0.18 | 0.28 |
| $[CTA]_0$ / $[V\text{-}50]_0$ | 15.80 | 7.17 | 9.34 | 6.10 | 7.82 | 5.44 | 6.78 | 4.91 | 5.97 |

**Supplementary Table 3 | Preparation conditions of P($DMA_{250}$-*b*-$AMPS_{150}$-*b*-$DMA_{250}$-*b*-$AMPS_{150}$-*b*-$DMA_{250}$) and P($DMA_{250}$-*b*-$AMPS_{150}$-*b*-$DMA_{250}$-*b*-$AMPS_{150}$-*b*-$DMA_{250}$-*b*-$AMPS_{150}$-*b*-$DMA_{250}$-*b*-$AMPS_{150}$-*b*-$DMA_{250}$) synthesized via the one-pot RAFT polymerization in a 10-mM phosphate buffer solution at 70 °C with V-50 initiator (2 h per block).** [a] Represents the sum of the total volume of monomer + volume of initiator stock solution + volume of solvent + $V_{total}$ from the previous block. [b] $m_{v\text{-}50\ total}$ represents the sum of the initiator added $m_{v\text{-}50\ added}$ + the amount of initiator remaining from the previous block $m_{v\text{-}50\ remaining}$. ($m_{v\text{-}50\ remaining} = m_{v\text{-}50\ total} \times 2f e^{-k_d t} \times (1\text{-}f_c/2)$ with $f$ = 0.5, $f_c$ = 0,[S8] $k_d$ = $1.21 \times 10^{-4}$ $s^{-1}$.[S9]

| Block | Polymer | Monomer conversion[a] (%) | $M_{n,th}$[b] (g mol$^{-1}$) | $M_{n,GPC}$[c] (g mol$^{-1}$) | $Đ$[c] |
|---|---|---|---|---|---|
| 1 | Poly(DMA$_{250}$) | > 99 | 25,090 | 18,118 | 1.04 |
| 2 | Poly(DMA$_{250}$-*b*-AMPS$_{150}$) | > 99 | 59,474 | 42,567 | 1.26 |
| 3 | Poly(DMA$_{250}$-*b*-AMPS$_{150}$-*b*-DMA$_{250}$) | 99 | 84,257 | 65,005 | 1.38 |
| 4 | Poly(DMA$_{250}$-*b*-AMPS$_{150}$-*b*-DMA$_{250}$-*b*-AMPS$_{150}$) | > 99 | 118,641 | 85,480 | 1.45 |
| 5 | Poly(DMA$_{250}$-*b*-AMPS$_{150}$-*b*-DMA$_{250}$-*b*-AMPS$_{150}$-*b*-DMA$_{250}$) | 99 | 143,424 | 114,975 | 1.54 |
| 6 | Poly(DMA$_{250}$-*b*-AMPS$_{150}$-*b*-DMA$_{250}$-*b*-AMPS$_{150}$-*b*-DMA$_{250}$-*b*-AMPS$_{150}$) | 99 | 177,808 | 131,623 | 1.64 |
| 7 | Poly(DMA$_{250}$-*b*-AMPS$_{150}$-*b*-DMA$_{250}$-*b*-AMPS$_{150}$-*b*-DMA$_{250}$-*b*-AMPS$_{150}$-*b*-DMA$_{250}$) | 98 | 202,591 | 152,098 | 1.81 |
| 8 | Poly(DMA$_{250}$-*b*-AMPS$_{150}$-*b*-DMA$_{250}$-*b*-AMPS$_{150}$-*b*-DMA$_{250}$-*b*-AMPS$_{150}$-*b*-DMA$_{250}$-*b*-AMPS$_{150}$) | > 99 | 236,975 | 163,212 | 1.90 |
| 9 | Poly(DMA$_{250}$-*b*-AMPS$_{150}$-*b*-DMA$_{250}$-*b*-AMPS$_{150}$-*b*-DMA$_{250}$-*b*-AMPS$_{150}$-*b*-DMA$_{250}$-*b*-AMPS$_{150}$-*b*-DMA$_{250}$) | 99 | 261,757 | 186,242 | 1.97 |

**Supplementary Table 4 | Final conversions, number-average molar masses, and dispersity values of P(DMA$_{250}$-*b*-AMPS$_{150}$-*b*-DMA$_{250}$-*b*-AMPS$_{150}$-*b*-DMA$_{250}$) and P(DMA$_{250}$-*b*-AMPS$_{150}$-*b*-DMA$_{250}$-*b*-AMPS$_{150}$-*b*-DMA$_{250}$-*b*-AMPS$_{150}$-*b*-DMA$_{250}$-*b*-AMPS$_{150}$-*b*-DMA$_{250}$) obtained in this study.** [a] Determined by $^1$H NMR. [b] Determined using eq (1). [c] Determined using GPC.

| Cycle | 1 | 2 | 3 |
|---|---|---|---|
| Monomer | APTC | DMA | APTC |
| $DP_{targeted}$ | 150 | 750 | 150 |
| $m_{Monomer\ added}$ (mg) | 1805 | 4125 | 1805 |
| $m_{CTA\ added}$ (mg) | 17.9 | - | - |
| $m_{V\text{-}50\ added}$ (mg) | 3.5 | 3 | 4 |
| $V_{PB\ added}$ (mL) | 6 | 10 | 3 |
| $V_{total}$ (mL)[a] | 8.868 | 23.758 | 29.726 |
| $m_{V\text{-}50\ total}$ (mg)[b] | 3.5 | 3.7 | 4.74 |
| $[V\text{-}50]_0$ (mol/L) | $1.46 \times 10^{-3}$ | $5.74 \times 10^{-4}$ | $5.87 \times 10^{-4}$ |
| $[Monomer]_0$ (mol/L) | 0.98 | 1.75 | 0.29 |
| $[CTA]_0 / [V\text{-}50]_0$ | 4.51 | 4.26 | 3.33 |

**Supplementary Table 5 | Preparation conditions of P($APTC_{150}$-*b*-$DMA_{750}$-*b*-$APTC_{150}$) synthesized via the one-pot RAFT polymerization in a 10-mM phosphate buffer solution at 70 °C with V-50 initiator (2 h per block).** [a] Represents the sum of the total volume of monomer + volume of initiator stock solution + volume of solvent + $V_{total}$ from the previous block. [b] $m_{v\text{-}50\ total}$ represents the sum of the initiator added $m_{v\text{-}50\ added}$ + the amount of initiator remaining from the previous block $m_{v\text{-}50\ remaining}$. ($m_{v\text{-}50\ remaining} = m_{v\text{-}50\ total} \times 2f e^{-kdt} \times (1\text{-}f_c/2)$ with $f = 0.5$, $f_c = 0$,[S8] $k_d = 1.21 \times 10^{-4}\ s^{-1}$.[S9]

| Block | Polymer | Monomer conversion[a] (%) | $M_{n,th}$[b] (g mol$^{-1}$) | $M_{n,GPC}$[c] (g mol$^{-1}$) | $Đ$[c] |
|---|---|---|---|---|---|
| 1 | Poly(APTC$_{150}$) | > 99 | 31,314 | 16,392 | 1.12 |
| 2 | Poly(APTC$_{150}$-*b*-DMA$_{750}$) | 99 | 105,661 | 62,433 | 1.24 |
| 3 | Poly(APTC$_{150}$-*b*-DMA$_{750}$-*b*-APTC$_{150}$) | 99 | 136,668 | 78,365 | 1.29 |

**Supplementary Table 6 | Final conversions, number-average molar masses, and dispersity values of P(APTC$_{150}$-*b*-DMA$_{750}$-*b*-APTC$_{150}$) obtained in this study.** [a] Determined by $^{1}$H NMR. [b] Determined using eq (1). [c] Determined using GPC.

| Cycle | 1 | 2 | 3 |
|---|---|---|---|
| Monomer | AMPS | DMA | AMPS |
| $DP_{targeted}$ | 150 | 750 | 150 |
| $m_{Monomer\ added}$ (mg) | 1725 | 4125 | 1725 |
| $m_{CTA\ added}$ (mg) | 17.9 | - | - |
| $m_{V\text{-}50\ added}$ (mg) | 2 | 3 | 2.5 |
| $V_{PB\ added}$ (mL) | 6 | 10 | 3 |
| $V_{total}$ (mL)[a] | 9.565 | 24.455 | 31.07 |
| $m_{V\text{-}50\ total}$ (mg)[b] | 2 | 3.4 | 3.18 |
| $[V\text{-}50]_0$ (mol/L) | $7.71 \times 10^{-4}$ | $5.12 \times 10^{-4}$ | $3.77 \times 10^{-4}$ |
| $[Monomer]_0$ (mol/L) | 0.87 | 1.70 | 0.27 |
| $[CTA]_0 / [V\text{-}50]_0$ | 7.90 | 4.64 | 4.97 |

**Supplementary Table 7 | Preparation conditions of P(AMPS$_{150}$-*b*-DMA$_{750}$-*b*-AMPS$_{150}$) synthesized via the one-pot RAFT polymerization in a 10-mM phosphate buffer solution at 70 °C with V-50 initiator (2 h per block).** [a] Represents the sum of the total volume of monomer + volume of initiator stock solution + volume of solvent + $V_{total}$ from the previous block. [b] $m_{v\text{-}50\ total}$ represents the sum of the initiator added $m_{v\text{-}50\ added}$ + the amount of initiator remaining from the previous block $m_{v\text{-}50\ remaining}$. ($m_{v\text{-}50\ remaining} = m_{v\text{-}50\ total} \times 2f e^{-k_d t} \times (1\text{-}f_c/2)$ with $f = 0.5$, $f_c = 0$,[S8] $k_d = 1.21 \times 10^{-4}\ s^{-1}$.[S9]

| Block | Polymer | Monomer conversion[a] (%) | $M_{n,th}$[b] (g mol$^{-1}$) | $M_{n,GPC}$[c] (g mol$^{-1}$) | $Đ$[c] |
|---|---|---|---|---|---|
| 1 | Poly(AMPS$_{150}$) | > 99 | 34,692 | 29,805 | 1.12 |
| 2 | Poly(AMPS$_{150}$-*b*-DMA$_{750}$) | 99 | 109,039 | 93,755 | 1.16 |
| 3 | Poly(AMPS$_{150}$-*b*-DMA$_{750}$-*b*-AMPS$_{150}$) | 99 | 143,424 | 108,815 | 1.21 |

584

585 **Supplementary Table 8 | Final conversions, number-average molar masses, and dispersity values**
586 **of P(AMPS$_{150}$-*b*-DMA$_{750}$-*b*-AMPS$_{150}$) obtained in this study.** [a] Determined by $^{1}$H NMR. [b]
587 Determined using eq (1). [c] Determined using GPC.

588

589

590

591

592

593

594

595

596

597

598

599

600

601

602

603

## 11. Captions for Movies

**Movie S1.** CGMD simulation of tri-PEs network self-assembly: the yellow, blue and red monomers of polymers represent the neutral, negatively charged and positively charged species, respectively. (movie time 00:20)

**Movie S2.** CGMD simulation of penta-PEs network self-assembly: the yellow, blue and red monomers of polymers represent the neutral, negatively charged and positively charged species, respectively. (movie time 00:22)

**Movie S3.** CGMD simulation of nona-PEs network self-assembly: the yellow, blue and red monomers of polymers represent the neutral, negatively charged and positively charged species, respectively. (movie time 00:22)

**Movie S4.** The tri-PEC illustration through cluster analysis (here the coordinates of the monomers are unwrapped), independent PECs are shown with different colors. (movie time 00:21)

**Movie S5.** The penta-PEC illustration through cluster analysis (here the coordinates of the monomers are unwrapped), independent PECs are shown with different colors. (movie time 00:20)

**Movie S6.** The nona-PEC illustration through cluster analysis (here the coordinates of the monomers are unwrapped), independent PECs are shown with different colors. (movie time 00:22)

## 12. Supplementary References


S1. Grest, G. S., K. Kremer. *Phys. Rev. A*, 33, 3628 (1986).

S2. Kremer, K., G. S. Grest. *J. Chem. Phys.*, 92, 5057 (1990).

S3. Weeks, J. D., D. Chandler, H. C. Andersen. *J. Chem. Phys.*, **54**, 5437 (1971).

S4. Debye, P. Hückel, E. *Physikalische Zeitschrift*, **24**, 185 (1923).

S5. Thompson, A. P., H. M. Aktulga, R. Berger, D. S. Bolintineanu, W. M. Brown, P. S. Crozier, P. J. in 't Veld, A. Kohlmeyer, S. G. Moore, T. D. Nguyen, R. Shan, M. J. Stevens, J. Tranchida, C. Trott, S. J. Plimpton. *Comput. Phys. Commun.*, **271**, 108171 (2022).

S6. Evans, D., Morriss, G. Non-Equilibrium Statistical Mechanics of Liquids, Cambridge University Press, (2008).

S7. Todd and Daivis, Nonequilibrium Molecular Dynamics (book), Cambridge University Press, (2017).

S8. Gody, G., T. Maschmeyer, P. B. Zetterlund, S. Perrier. *Nat. Commun.*, **4**, 1 (2013).

S9. Yang, Z., H. Peng, W. Wang, T. Liu. *J. Appl. Polym. Sci.*, **116**, 2658 (2010).